Heterogeneity of the electrostatic repulsion between colloids at the oil–water interface

Bum Jun Park,[a] Jan Vermant[b] and Eric M. Furst*[a]

Received 8th June 2010, Accepted 14th August 2010
DOI: 10.1039/c0sm00485e

The pairwise and multi-body interaction forces between polystyrene particles at an oil–water interface are measured. The electrostatic repulsive force has the expected dependence on particle separation for a dipole–dipole interaction, $F_{rep} \sim r^{-4}$, but exhibits a distribution of magnitudes in which the force depends on the particle pairs tested and sample preparation method. A gamma distribution accurately models this variation in the repulsion between pairs of particles. Despite this heterogeneity, the multibody interactions measured in small ensembles are pairwise additive. Good agreement is found for the two-dimensional equilibrium suspension structure between experiments and Monte Carlo simulations when a heterogeneous interaction potential is implemented in the latter. The heterogeneity and long-range of the repulsive interaction accounts for the lower apparent pair interaction potential derived from the suspension radial distribution function at dilute, but finite, surface concentrations when compared to the direct pair interaction measurements made with laser tweezers at nearly infinite dilution.

1 Introduction

Electrostatic interactions are ubiquitous in soft matter, and play a significant role in phenomena as diverse as protein–protein interactions[1] and the kinetic stability of Faraday's gold sols.[2] The electrostatic interaction between colloidal particles dispersed in fluids has long been described by the Gouy–Chapman theory, in which charges are screened by a double layer of counter-ions.[3,4] In contrast, electrostatic interactions between charged particles at an oil–water interface are significantly stronger and surprisingly long ranged, as illustrated in Fig. 1. Particles that normally exhibit repulsion at separations on the order of one hundred nanometres when dispersed in the bulk will repel each other strongly at micrometre separations at the interface.

Pieranski first suggested that the repulsion is due to the strong electric field through the nonpolar phase caused by dipoles perpendicular to the fluid interface.[5] The dipoles arise due to the charge dissociation in the polar, aqueous phase. Based on this idea, Hurd proposed a dipole–dipole interaction model due to the separation of charge between the particle surface and the diffuse double layer.[6] The dipole strength is determined by both the point charge, which is the sum of dissociated surface charges in the aqueous phase, and the Debye screening length κ^{-1}. From the linearized Poisson–Boltzmann (P-B) equation, the repulsive force in the far field is expected to decay as the fourth power of the separation between the particles, $F_{rep} \sim 1/r^4$, in agreement with Pieranski's hypothesis.

Aveyard and coworkers later questioned the role of charge dissociation in the aqueous phase when their experiments, which directly measured the particle pair interaction forces, suggested that the electrostatic repulsion was independent of the salt concentration in the aqueous sub-phase, yet consistent with a dipole–dipole repulsion.[7,8] This implied that there was no screening effect, which was predicted in the Hurd model to scale as the inverse Debye screening length squared, $F_{rep} \sim \kappa^{-2}$. Alternatively, it was hypothesized that the repulsion arises from the presence of a small amount of charge on the particles in the *oil* phase, possibly due to surface residual charges stabilized by water molecules trapped at the rough particle surface. This would give rise to unscreened Coulomb interactions through the oil phase. In such a case, the long-range repulsive force also scales as r^{-4}, but is independent of the screening length in the aqueous phase, since this model only considers charges in the oil phase.

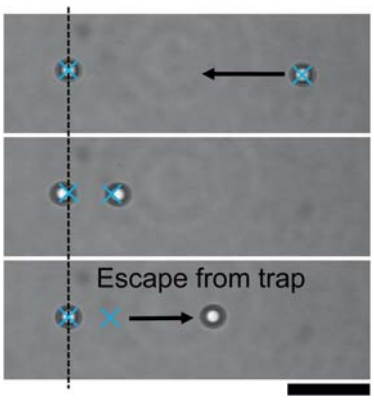

Fig. 1 Example of the long-range repulsive interaction between colloids pinned at the oil–water interface. Two particles are brought together using time-shared optical traps by translating one of the particles. The deflection of stationary particle in its trap shows the repulsive force. When the repulsion exceeds the maximum trapping force generated by the optical tweezer, approximately 1 pN in this case, the translating particle is pushed away. The scale bar is 10 μm.

[a]*Department of Chemical Engineering and Center for Molecular and Engineering Thermodynamics, University of Delaware, 150 Academy Street, Newark, Delaware, 19716, U.S.A. E-mail: furst@udel.edu; Fax: +1 302 831 1048; Tel: +1 302 831 0102*
[b]*Department of Chemical Engineering, K. U. Leuven, W. de Croylaan 46, B-3001 Leuven, Belgium*

Three recent developments resolved the mechanism of electrostatic interactions between colloids at the oil–water interface and confirmed the general principle of Hurd that charge dissociation in the aqueous phase leads to the long-range dipolar repulsion. First, additional experiments revealed that the repulsion is *weakly*, but non-negligibly, dependent on salt concentration, and that the repulsive force scales as $F_{rep} \sim \kappa^{-0.43 \pm 0.04}$ when monovalent salts like sodium chloride are present in the aqueous sub-phase.[9] Second, Hurd's theory was corrected to account for charge renormalization due to the highly non-linear counterion distribution and resulting dense counterion layer at the particle surface expected for highly-charged particles.[10] This explained the weak dependence on the screening length, predicting that $F_{rep} \sim \kappa^{-0.8 \cdots -0.4}$. Unfortunately, however, the magnitude of the repulsion remained unresolved, with up to several orders of magnitude difference between theory and measurements.[11] To complicate matters, this quantitative discrepancy could not be adequately addressed at the time due to a fairly wide range of magnitudes reported from a number of experimental studies using different techniques.[12] Finally, Masschaele *et al.* employed several experimental approaches in a single study, including characterization of the equilibrium static and dynamic structure, laser tweezers and surface rheology measurements, to establish consistent measurements.[13] Furthermore, they proposed that the finite thickness of the Stern layer provides the dominant (and previously neglected) contribution to the dipole strength that *quantitatively* accounts for the magnitude of the consensus experimental measurements.

Despite this progress in the measurement and understanding of electrostatic interactions at the oil–water interface, there remain a number of important aspects left to address. In previous work, we noted that the strength of repulsion between particle pairs at the oil–water interface is *heterogeneous*.[9] The magnitude of the repulsive force varies depending on the individual particles and particle pair used in each force measurement. In this paper, we examine the distribution of repulsive interactions between particles at the oil–water interface in detail, and discuss the important implications it has on the methods used to characterize the potential. Specifically, we compare pair interaction measurements at infinite dilution using laser tweezers to the interaction potential extracted from the equilibrium structure of two-dimensional suspensions at the oil–water interface. Second, we examine the effect of sample preparation protocols. Treating particles by multiple centrifugation and redispersion steps in ultrapure water leads to significantly higher repulsive forces, and may account for some of the reported differences in the literature. Finally, we examine the consequences of heterogeneous interactions on the equilibrium structure of 2D suspensions and discuss potential shortcomings of extracting pair potentials from the radial distribution function. Before discussing these results, we first review the materials and methods used in this study.

2 Materials and methods

2.1 Pair interaction measurements

Our experimental geometry consists of an interface formed between water and decane. Ultra-purified water (resistivity > 18.2 MΩ·cm) is used as the sub-phase. The super-phase is *n*-decane (Acros Organics, 99+%), which has been passed through an aluminium oxide column (Acros Chemical, acidic activated, particle size 100–500 μm) to remove polar contaminants. The particles are surfactant-free, charge-stabilized polystyrene (PS) with sulfate groups (surface charge density, $\sigma = 7.4$ μC/cm^2) and diameter $2a = 3.1 \pm 0.2$ μm (Invitrogen Corporation, Carlsbad, CA). In this study, particles are washed by multiple (≥7) centrifugation and redispersion steps. Isopropyl alcohol (Sigma Aldrich) is used as the spreading solvent to introduce the particles into the interface.[9,14] The interfacial tension of the oil–water interface $\gamma_{OW} \approx 50$ mN/m is measured by a pendant drop technique,[14,15] while the three-phase contact angle was reported by Masschaele *et al.*[13] as $\theta_c = 90 \pm 20°$.

A specially fabricated fluid cell (Fig. 2), consisting of a glass outer cylinder and an inner cylinder made of aluminium, is placed on the stage of an inverted microscope (Zeiss Axiovert 200). The outer cylinder is attached to a 40 mm circular coverglass (No. 1.5 Fisherbrand) using UV curing epoxy (Norland Products, NOA 81). A teflon ring is inserted into the bottom of the inner cylinder in order to pin the contact line of the oil–water interface. The glass spacer provides a path for water to exchange between the thin water film and the outer cylinder. In order to prevent evaporation of water and convection at the interface, the container is sealed with vacuum grease. All glassware is cleaned using a plasma cleaner (Harrick Plasma, PDC 32-G), immediately before constructing the cell to achieve good wetting conditions for the water.

Particles at the interface are trapped by time-shared optical traps in the same manner of Pantina and Furst.[16] Drag calibration[9,16,17] where the particle position is measured as a function of drag forces imposed by the fluid at a constant velocity, is used to calibrate the optical trap stiffness κ_t. We confirm the trap stiffness by measuring the thermal fluctuations of the particle in the optical trap. Pair interaction forces are directly measured as one particle is translated step-wise toward another stationary particle.[9] The particle displacement in the stationary trap provides a quantitative measurement of the forces exerted between the two particles, as shown in Fig. 1. The particles are initially trapped with a large separation such that the interaction between them is negligible.

There are several potential artifacts in laser tweezer experiments, including thermocapillary forces[18] and radiation pressure forces.[19] We recently evaluated the trapping forces at the oil–water interface.[17] One particular concern, for instance, is that

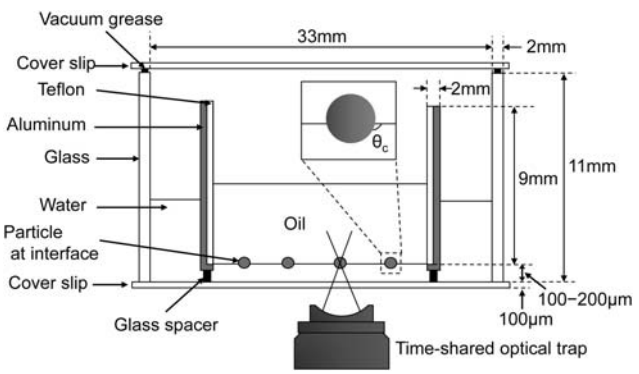

Fig. 2 Schematic of the experimental geometry.

the radiation pressure is sufficiently strong to displace the particle normal to the interface, thus deforming the interface and leading to capillary attraction between particles. We verified that there are no such artifacts in the pair potential measurements at the laser powers we use. Furthermore, interactions were validated using "passive" measurements using a particle trajectory analysis. Particles are brought to a finite separation using the traps, then the laser is shuttered. The force at each separation is related to the measured drift velocity v by

$$F_{\text{rep}} = 6\pi a \eta_{\text{eff}} v \tag{1}$$

where effective viscosity is a function of both the oil and water phase viscosities, $\eta_{\text{eff}} = [\eta_{\text{oil}}(1 - \cos\theta) + \eta_{\text{water}}(1 + \cos\theta)]/2$.

Pair interaction measurements using laser tweezers are compared in this study to the interaction potential determined from the equilibrium radial distribution function (RDF), $g(r)$. Briefly, particles are spread at the oil–water interface as described above, but at higher (but still dilute) surface fraction ρ. Image frames of the suspension are captured and analyzed using particle tracking.[20] The two-dimensional (2D) radial distribution function is calculated as,

$$g(r_\lambda) = \frac{\langle N_\lambda \rangle}{2\pi N \rho_N r_\lambda dr} \tag{2}$$

where N is the total number of particles, $\langle N_\lambda \rangle$ is the number of particles in the interval r_λ to $r_{\lambda+1} = r_\lambda + dr$ and ρ_N is the particle number density per unit area. Note that the latter quantity is related to the surface area fraction by $\rho_N = \rho/\pi a^2$. The potential of mean force is[21]

$$w(r) = -k_B T \ln g(r). \tag{3}$$

At sufficiently low area fractions, the potential of mean force can be approximated by the pair potential $U(r)$ and thus is often calculated from the radial distribution function under dilute conditions,[13]

$$U(r) = -\lim_{\rho \to 0} k_B T \ln g(r).$$

2.2 Monte Carlo simulations

Metropolis Monte Carlo (MC) is used to compare the equilibrium suspension structure found in experiments to the structure obtained using model interaction potentials. This enables us to quantitatively analyze the role of heterogeneity in the pair potential on the structure and understand the potential bias of interaction potentials obtained from measurements of "dilute" suspensions. In the simulations, N particles in two dimensions are assumed to interact with each other *via* the dipole–dipole repulsive interaction given by,

$$\frac{U_{ij}}{k_B T} = (a_{2,i} + a_{2,j})\frac{1}{r_{ij}^3} = a_{2,ij}\frac{1}{r_{ij}^3}, \tag{5}$$

where k_B is the Boltzmann's constant, T is the temperature, and each particle (i, j) carries its own half-pair potential $(a_{2,i}, a_{2,j})$, and its sum $(a_{2,i} + a_{2,j})$ corresponds to the pair interaction prefactor $a_{2,ij}$ between particles i and j. The force measured using optical tweezers is assumed to be conservative and thus related to this potential by

$$F_{\text{rep}} = -\frac{dU}{dr} = \frac{3a_{2,ij}k_B T}{r_{ij}^4}. \tag{6}$$

Assuming pairwise additive potentials,[22] the total energy used to determine whether to accept or reject a new configuration after particle i is randomly moved is the sum of all pair interactions with its neighboring particles j,

$$U_{tot} = \sum_j^N U_{ij} \quad (i \neq j). \tag{7}$$

(U_{tot} may not be identical to the total energy of the system due to the possible contributions of many-body interactions,[23] a phenomenon which we evaluate later.)

In order to investigate the effect of heterogeneous repulsive interactions in the simulation, we compare single values of the pair interaction prefactor for all particles (*i.e.*, $a_{2,i} = a_{2,j} = a_2/2$) to a distribution of values based on the experimental measurements. Initial particle positions are obtained from an image analysis of an experiment[20] and each is randomly moved with a radial step size $dr = 0.5$ μm. We conduct 10^4 simulation cycles to obtain the simulated radial distribution function (RDF) at a given condition and each cycle includes N MC cycles for N particle movements. After reaching an equilibrium where the average spacing $< L >$ between particles plateaus, each particle position during 5000 simulation cycles is saved to calculate the RDF. The deviation of the simulated RDF (g_{MC}) from the experiment g_{exp} is defined by,[22]

$$\chi^2 = \frac{1}{m}\sum_{k=1}^{m}\left\{\frac{g_{MC}(r_k) - g_{exp}(r_k)}{\sigma_k}\right\}^2 \quad k = 1, 2, \ldots, m, \tag{8}$$

where m is the number of discrete points used to evaluate the distribution functions.

3 Results and discussion

3.1 Pair interaction measurements

Laser tweezers are used to directly measure the interaction force between particle pairs at a pure oil–water interface. As shown in Fig. 3, the interaction is dominated by the electrostatic dipolar repulsion in the far field, consistent with previous results.[7,9] Note the long range of the repulsion–particles repel with forces up to 2 pN even when separated by a distance of 2–7 μm, or approximately 1–3 particle diameters.

Consistent with our previous study, the repulsive interactions vary substantially depending on the particle pairs that are measured.[9] The force profiles in Fig. 3a, measured for 32 separate particle pairs, show a broad distribution. We fit each measured interaction potential with the dipolar force expression (eqn (6)) to determine the interaction prefactor a_2. The prefactor varies between $1.2 < a_2 \times 10^{13} < 12.2$ m^3 and has a mean value $\langle a_2 \rangle = 5.1 \pm 2.4 \times 10^{-13}$ m^3. This average is higher than the value $\langle a_2 \rangle = 1.3 \pm 0.5 \times 10^{-13}$m^3 reported in Masschaele *et al.*,[13] and is attributed to the introduction of particle washing *via* multiple centrifugation and redispersion steps in the sample preparation protocol. The higher repulsive force is also apparent by the fact

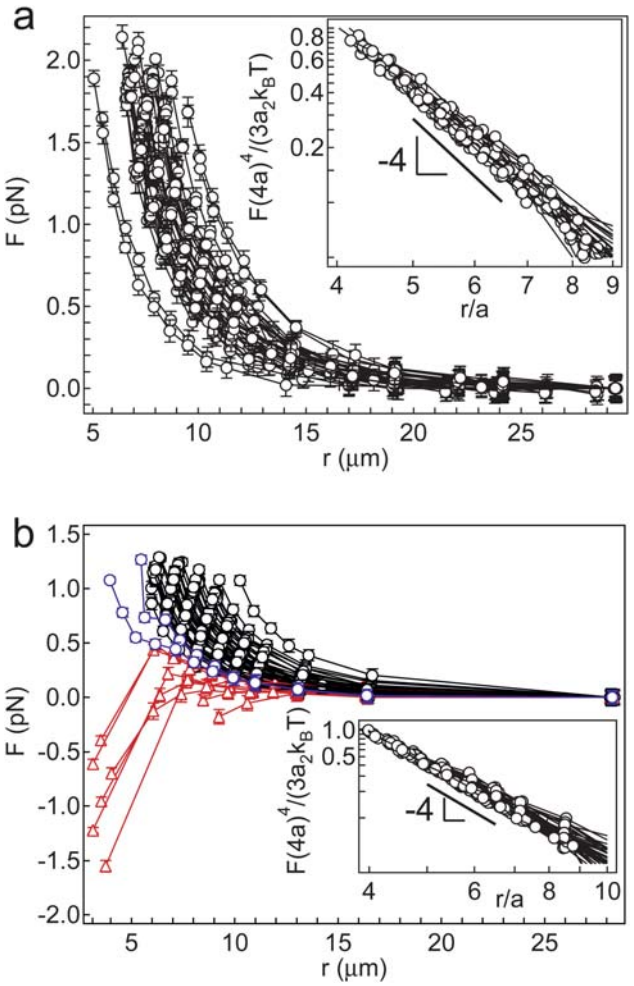

Fig. 3 Interaction force between two particles at a pure decane–water interface. The trap stiffness is $\kappa_t = 1.71 \pm 0.02$ pN/μm for washed particles (a) and $\kappa_t = 1.18 \pm 0.01$ pN/μm for unwashed particles (b). Blue curves are force profiles that deviate from the expected $F_{rep} \sim r^{-4}$ force law in the near field and red curves exhibit a near-field attraction that causes particles to "jump-in" to contact. The insets show log-log plots of the data normalized by the magnitude of the force and radius a. (Note that the inset in b only includes the repulsive pairs.) Fig. 4 shows the corresponding distribution of a_2 values used to scale the force data.

that none of the 32 measurements exhibit a near-field attraction, while 6 of 55 measurements of non-washed particles, shown in Fig. 3b, eventually exhibit a "jump-in" to contact.[13] In the latter case, the values of a_2 for interaction measurements that do not exhibit a near-field attraction vary between 0.5×10^{13} m^3 and 9×10^{13} m^3. Although the force profile for all of the repulsive curves exhibit a $1/r^4$ dependence in the far field (see the insets in Fig. 3a and b), more weakly interacting unwashed particles show some deviation in the near-field.

The distributions of a_2 values are shown in Fig. 4 for the washed and unwashed particles. The distributions are clearly skewed to lower values, with the highest frequency of a_2 values between $0.57–1.2 \times 10^{-13}$ m^3 for the unwashed particles and 3–4 $\times 10^{-13}$ m^3 for the washed particles. Although at this time we do not understand what causes differences between washed and unwashed particles (minute quantities of contaminants or

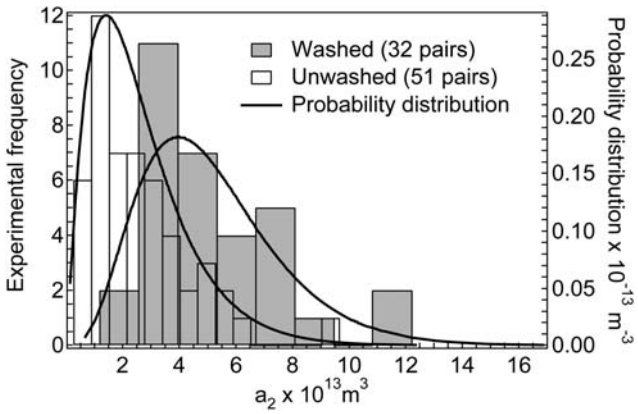

Fig. 4 Histogram for experimental pair potentials for 32 particle washed pairs (gray bars) and 51 unwashed pairs (transparent bars). The solid line is the corresponding normalized gamma distribution (right axis).

synthesis byproducts that are removed by the washing process are possible explanations), the skewed distributions are intriguingly similar to the distributions that characterize the charge nonuniformity of polystyrene latex particles in the absence of adsorbed species.[24] The measured charge nonuniformity is a result of local surface potentials that ranged as much as 50–75% of the average particle zeta potential.[25] Thus, the variation in repulsive forces captured by Fig. 4 could be due to the orientation of charged patches relative to the interface. If a highly charged patch by chance oriented downward into the aqueous

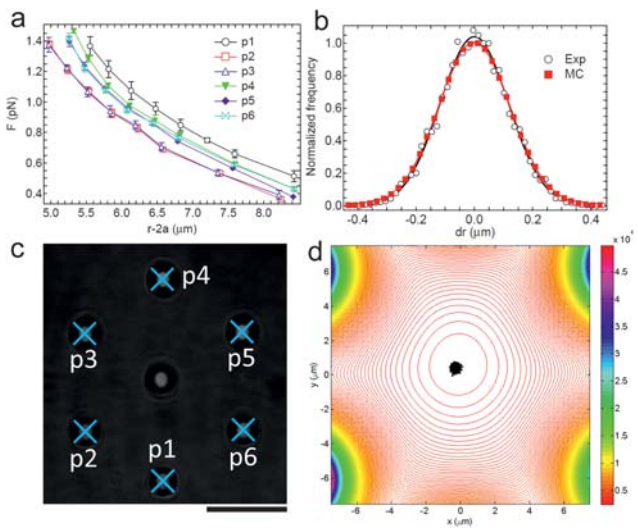

Fig. 5 Pairwise additivity. (a) Pair interactions; (b) Normalized Boltzmann distribution of the center particle trajectories. Open circle is experiment and red square is the Monte Carlo simulation with considering the pairwise interaction. The spring constant k_s is extracted as $k_{s,\,exp} = 73.0 \pm 2.5\ k_BT/\mu m^2$ and $k_{s,\,MC} = 66.6 \pm 0.2\ k_BT/\mu m^2$ using the Gaussian fitting $P(dr) = A\exp\dfrac{-k_s dr^2}{2k_BT}$ where dr is the radial displacement of the center particle; (c) Snapshot of the seven particle configuration. The scale bar is 10 μm; (d) Contour plot of the pairwise potential field. Black dots represents the experimental trajectories of the center particle.

phase and normal to the interface, then the repulsive interactions with other particles would be stronger.

Although the interaction potentials between particle pairs vary (sometimes considerably), we confirm that the interactions are pairwise additive. As shown in Fig. 5a, the pair interaction between a single particle and six other particles (P1–P6) were each measured independently. The six particles were then held by optical traps in a hexagonal pattern surrounding the "common" particle, which was allowed to diffuse freely in this cage (Fig. 5c). Fig. 5d shows that the average position of the central particle is in good agreement with the total potential calculated by assuming pairwise additivity of the pair potentials. Next, we examine how the heterogeneity on the pair interaction affects the suspension equilibrium structure, such as the radial distribution function, using Monte Carlo simulations.

3.2 Suspension structure

Recently, Masschaele *et al.* demonstrated that concurrent multiple experiments, including laser tweezers, equilibrium structure characterization, strain fluctuations and surface rheology, yield interaction potentials between colloids at the oil–water interface that are in *quantitative* agreement to within a factor of ~2–3, provided that the same colloidal suspension and identical preparation protocols are used.[13] Among the slight differences between experiments, laser tweezer measurements between particle pairs in the study yielded consistently higher repulsive interactions than those calculated from the equilibrium structure. The interaction prefactor $a_2 = 0.5 \pm 0.5 \times 10^{-13}$ m^3 was obtained from the radial distribution function at low surface fractions, while laser tweezer measurements gave $\langle a_2 \rangle = 1.3 \pm 0.5 \times 10^{-13}$ m^3, a factor of nearly three higher. While the average values differ, the prefactor derived from the radial distribution function clearly agrees with the lower range of values obtained using laser tweezers, as discussed in the previous section.

Given the role that experimental uncertainty has played in resolving the repulsive mechanism for particles at the oil–water interface, it is important to understand the origin of these differences, since it has been suggested that such inconsistencies reflect systematic errors of the experiments or calibration procedures.[12] Here, we show that radial distribution function measurements of the dipole–dipole interaction at low surface fractions are biased towards the lower magnitudes of the heterogeneous repulsion, a fact which extends beyond its application here to potentially any case in which the pair potential between colloidal particles is derived from the equilibrium radial distribution function. Second, we demonstrate that the *heterogeneous* pairwise dipole–dipole interactions are sufficient to explain the observed equilibrium structure for particles spread at the oil–water interface.

Monte Carlo simulations of the 2D suspension structure are performed as described in section 2. First, a pairwise potential is chosen to match the minimum and maximum values of the repulsion prefactors ($a_2 = a_{2,ij}$) obtained from radial distribution function measurements[13] and our laser tweezer experiments, respectively. The corresponding radial distribution functions, $g(r)$, are shown in Fig. 6a. The green line in Fig. 6a shows $g(r)$ at the maximum prefactor $a_2 = 5.1 \times 10^{-13}$ m^3, which results in a hexagonal crystal with significant peaks in the far field. The

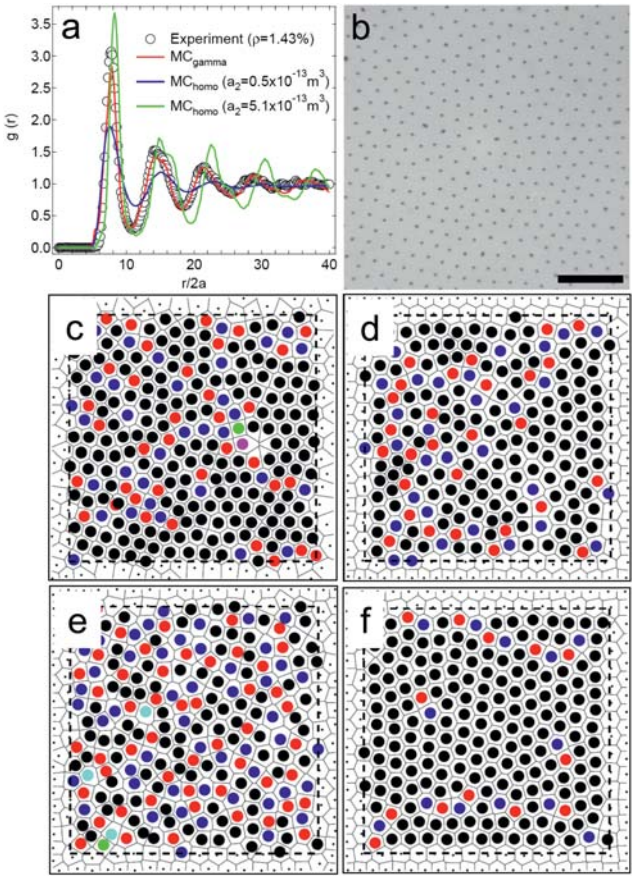

Fig. 6 The effect of repulsion magnitude a_2 and heterogeneity on the radial distribution function of a 2D colloidal suspension. (a) Comparison of radial distribution functions between the experiment and Monte Carlo simulations for two homogeneous interactions ($a_2 = 0.5 \times 10^{-13}$ and $a_2 = 5.1 \times 10^{-13}$ m^3) and a_2 values with a gamma distribution. (b) A snapshot of the hexagonal lattice of the colloidal suspension. The scale bar is 100 μm. Voronoi diagrams are shown for the (c) experiment, (d) MC simulations with a gamma distribution of a_2 values, (e) homogeneous repulsion with $a_2 = 0.5 \times 10^{-13}$, and (f) homogeneous repulsion with $a_2 = 5.1 \times 10^{-13}$ m^3. The color dots indicate particle positions. Black, red and blue correspond to particles with 6, 5 and 7 nearest neighbors.

corresponding Voronoi diagram, shown in Fig. 6f, exhibits few defects in the 6-fold symmetry. This ordered structure disappears when the lower bounding prefactor, $a_2 = 0.5 \times 10^{-13}$ m^3 is used in the MC simulation, as shown by the blue line in Fig. 6a and the Voronoi diagram in Fig. 6e. The large number of particles with 5 and 7 nearest neighbors is indicative of significant melting *via* the formation of dislocation pairs.[26,27] Notably, the radial distribution functions for both high and low values of a_2 deviate significantly from the experimentally obtained radial distribution function $g(r)$ (open symbols), corresponding to the snapshot in Fig. 6b where the surface coverage of particles is $\rho = 1.43\%$, the mean separation is $< L > = 25.2 \pm 3.3$ μm, and the number of particles is $N = 317$ in the interface area 409 × 409 μm^2.

In order to introduce a heterogeneous repulsion that captures the range of interaction measurements discussed in section 3.1, we assume that the prefactor a_2 varies. The experimental results for 32 pairs follow a gamma distribution with a shape parameter k and a scale parameter θ,

$$f(a_2;k,\theta) = a_2^{k-1}\frac{e^{-a_2/\theta}}{\theta^k \Gamma(k)}, \quad (9)$$

where $\Gamma(k)$ is the gamma function.[28] The fitted parameter values with 95% confidence intervals are $k = 4.42$ and $\theta = 1.16 \times 10^{-13}$ m^3 (Fig. 4), respectively, which are used for randomly generating half-pair potential prefactors ($a_{2,i}$, $a_{2,j}$). An advantage of the gamma distribution is that the sum of gamma random variables is also a gamma random variable; hence, this implies that $a_{2,i}$ and $a_{2,j}$ follow a gamma distribution, justifying the sum used in eqn (5). The introduction of this heterogeneous interaction potential based on the experimental tweezer measurements and gamma distribution leads to excellent agreement between the experimental and simulated radial distribution functions, as shown by the red line in Fig. 6a.

Consistent with the dependence of the radial distribution function on the interaction strength and heterogeneity, the fraction of particles with 5-, 6- and 7-fold nearest neighbors also shows the best agreement between MC simulations and experiment when the simulations incorporate the distribution of repulsive interaction strengths derived from the laser tweezer measurements. Table 1 summarizes the bond number distributions. In all cases, the number of particles with 5 and 7 neighbors is equal, consistent with the formation of dislocation pairs; however, at low and high values of a_2, the simulations exhibit more and fewer dislocations than the experiment, respectively.

Table 1 Comparison of the fraction of particles with bond numbers from 5–7 between experiment and three Monte Carlo (MC) simulations

	Bond number		
	5	6	7
Experiment	0.16	0.70	0.14
MC, gamma distribution	0.14	0.70	0.16
MC, $a_2 = 0.5 \times 10^{-13}$ m^3	0.25	0.48	0.25
MC, $a_2 = 5.1 \times 10^{-13}$ m^3	0.07	0.86	0.07

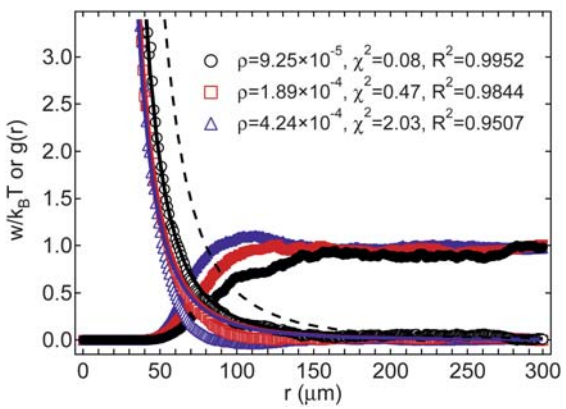

Fig. 7 The radial distribution function (closed symbols) and corresponding potential of mean force $w(r)$ (open symbols) from Monte Carlo simulations in the dilute regime with $a_2 = 5.1 \times 10^{-13}$ m^3 for three particle area fractions. Solid lines show fits of the dipole–dipole interaction potential (eqn (5)) to the potential of mean force. Although $w(r)$ is nearly identical in functional form to the pair potential at $\rho = 0.00925\%$, the *apparent* magnitude of the interaction is weaker.

Clearly, from the above comparison between experiment and MC simulations, a heterogeneous interaction potential must be employed to quantitatively match the equilibrium structure. This in part explains the lower values of a_2 derived from the radial distribution function of dilute suspensions when compared to laser tweezer measurements. The stronger repulsion between a small fraction of particles (represented by the upper tail of the gamma distribution) causes the more weakly interacting particles to be pushed closer together; thus, from the radial distribution function, the repulsive interaction would appear to be weaker when eqn (4) is used. In fact, a similar issue would likely occur regardless of whether the repulsion is heterogeneous or not due to difficulty establishing the limit of dilute interactions for such strongly repulsive interactions while still maintaining sufficient realizations of the particle positions to accurately calculate the radial distribution function.

We illustrate the subtlety of determining the pair potential from the radial distribution function with further MC simulation results. At low concentrations, the potential of mean force exhibits features characteristic of the fluid structure, such as a shallow, long-range well that corresponds to the emergence of a weak peak in $g(r)$, as shown in Fig. 7 for $\rho = 0.0424\%$. Clearly, the potential of mean force $w(r)$ would not be mistaken for the long-range dipolar interaction, which is the pair potential used in the simulation; the dipole–dipole interaction potential (eqn (5)) is a poor fit to $w(r)$, as shown by the solid blue curve. However, as the area fraction decreases, the $g(r)$ becomes increasingly monotonic. At $\rho = 0.00925\%$, the fit of eqn (5) to $w(r)$ is excellent, but the apparent magnitude of the interaction is lower by a factor of 2 from the input potential, shown by the dashed line. Physically, this is because the *apparent* interaction between a pair of particles also includes the effect of the remaining N–2 particles as they are canonically averaged over all configurations.[21] Thus, any two particles are "pushed together" by the remaining N–2 particles, giving the appearance of a weaker pair potential.

4 Conclusions

In this paper, we examined the distribution of repulsive interactions between particles at the oil–water interface. The magnitude of the repulsive interaction varies depending on the particles used in the pairwise measurement. Moreover, "washing" the particles with several cycles of centrifugation and redispersion increases the magnitude of the repulsion to the point that few, if any, pairs exhibit an attractive interaction at closer separations. In both cases, the distribution of the repulsive interaction could be accurately described by a gamma distribution. Despite the heterogeneity of the repulsion, the multibody forces are pairwise additive.

The heterogeneity of the repulsive interaction elucidated by pair measurements using laser tweezers suggests an explanation for the remaining variability of a_2 derived from the various experimental methods. After properly accounting for heterogeneity, the equilibrium suspension structure could be accurately calculated using Monte Carlo simulations. The presence of some particles with higher repulsive interactions likely biases the radial distribution function of more weakly interacting particles to give an apparent, weaker potential. Our results also highlight the difficulty in obtaining sufficiently low concentrations such that

the potential of mean force is asymptotically equal to the pair potential, $\lim_{\rho\to 0} w(r) = U(r)$ when the interactions exhibit such long range. While the particle area fraction is small, the *effective* area fraction is much larger. For instance, estimating the effective particle radius as the particle separation when $U(r) = k_BT$ for $a_2 = 5.1 \times 10^{-13}$ m^3 (the value used in Fig. 7) yields $a_{eff}/a \approx 27$ and an effective area fraction $\rho_{eff} = \rho(a_{eff}/a)^2 \approx 7\%$. But without *a priori* knowledge of the interaction magnitude, it is difficult to establish the area fraction ρ that will yield sufficiently dilute conditions to measure $U(r)$ directly.

A clear understanding of the pair interaction potential, including its magnitude and its heterogeneity, should be useful for simulations of two-dimensional suspensions, especially when modeling their structure, stability and surface rheology. A major remaining question is the nature of the attractive interaction observed for more weakly repulsive particles and whether this also exhibits heterogeneity.

We gratefully acknowledge helpful discussions with B. Ogunnaike, K. Masschaele and P. Lele and financial support from the National Science Foundation (NSF CBET-0553656) and the EU Erasmus Mundus program (EMF).

References

1 P. S. Stayton and S. G. Sligar, *Biochemistry*, 1990, **29**, 7381–7386.
2 M. Faraday, *Philos. Trans. R. Soc. London*, 1857, **147**, 145–181.
3 G. Gouy, *J. Phys. Radium*, 1910, **9**, 457–468.
4 D. L. Chapman, *Phil. Mag.*, 1913, **25**, 475–481.
5 P. Pieranski, *Phys. Rev. Lett.*, 1980, **45**, 569–572.
6 A. J. Hurd, *J. Phys. A: Math. Gen.*, 1985, **18**, L1055–L1060.
7 R. Aveyard, J. H. Clint, D. Nees and V. N. Paunov, *Langmuir*, 2000, **16**, 1969–1979.
8 R. Aveyard, B. P. Binks, J. H. Clint, P. D. I. Fletcher, T. S. Horozov, B. Neumann, V. N. Paunov, J. Annesley, S. W. Botchway, D. Nees, A. W. Parker, A. D. Ward and A. N. Bergess, *Phys. Rev. Lett.*, 2002, **88**, 246102.
9 B. J. Park, J. P. Pantina, E. M. Furst, M. Oettel, S. Reynaert and J. Vermant, *Langmuir*, 2008, **24**, 1686–1694.
10 D. Frydel, S. Dietrich and M. Oettel, *Phys. Rev. Lett.*, 2007, **99**, 118302–4.
11 M. Oettel, A. Dominguez and S. Dietrich, *Phys. Rev. E: Stat., Nonlinear, Soft Matter Phys.*, 2005, **71**, 051401–16.
12 M. Oettel and S. Dietrich, *Langmuir*, 2008, **24**, 1425–1441.
13 K. Masschaele, B. J. Park, J. Fransaer, E. M. Furst and J. Vermant, *Phys. Rev. Lett.*, 2010, **105**, 048303.
14 S. Reynaert, P. Moldenaers and J. Vermant, *Langmuir*, 2006, **22**, 4936–4945.
15 E. J. Stancik and G. G. Fuller, *Langmuir*, 2004, **20**, 4805–4808.
16 J. P. Pantina and E. M. Furst, *Langmuir*, 2004, **20**, 3940–3946.
17 B. J. Park and E. M. Furst, *Langmuir*, 2008, **24**, 13383–13392.
18 A. R. Dasgupta, A. S. Ahlawat and A. P. K. Gupta, *J. Opt. A*, 2007, **9**, S189–S195.
19 A. Ashkin, *Biophys. J.*, 1992, **61**, 569–582.
20 J. C. Crocker and E. R. Weeks, http://www.physics.emory.edu/~weeks/idl/index.html.
21 D. A. McQuarrie, *Statistical Mechanics*, University Science Books, 2nd edn, 2000.
22 S. Jain, S. Garde and K. Kumar, *Ind. Eng. Chem. Res.*, 2006, **45**, 5614–5618.
23 J. Dobnikar, M. Brunner, H.-H. von Grunberg and C. Bechinger, *Phys. Rev. E: Stat., Nonlinear, Soft Matter Phys.*, 2004, **69**, 031402–7.
24 J. D. Feick, N. Chukwumah, A. E. Noel and D. Velegol, *Langmuir*, 2004, **20**, 3090–3095.
25 J. D. Feick and D. Velegol, *Langmuir*, 2002, **18**, 3454–3458.
26 J. M. Kosterlitz and D. J. Thouless, *J. Phys. C: Solid State Phys.*, 1973, **6**, 1181.
27 K. Zahn, R. Lenke and G. Maret, *Phys. Rev. Lett.*, 1999, **82**, 2721–2724.
28 B. A. Ogunnaike, *Random Phenomena: Fundamentals of Probability and Statistics for Engineers*, CRC Press, 2009.